Modeling of nonlinear electron cyclotron resonance heating and current drive in a tokamak

Richard Kamendje
Institut für Theoretische Physik, Technische Universität Graz, Petersgasse 16, A-8010 Graz, Austria

Sergei V. Kasilov
*Institute of Plasma Physics, National Science Center "Kharkov Institute of Physics and Technology,"
Ul. Akademicheskaya 1, 61108 Kharkov, Ukraine*

Winfried Kernbichler
Institut für Theoretische Physik, Technische Universität Graz, Petersgasse 16, A-8010 Graz, Austria

Ivan V. Pavlenko
*EURATOM-Etat Belge, Université Libre de Bruxelles, Campus Plaine—CP 231, Boulevard du Triomphe,
B-1050 Bruxelles, Belgium*

Emanuele Poli
Max-Planck-Institut für Plasmaphysik, Bolztmannstrasse 2, D-85740 Garching bei München, Germany

Martin F. Heyn
Institut für Theoretische Physik, Technische Universität Graz, Petersgasse 16, A-8010 Graz, Austria

Electron cyclotron resonance heating and current drive are modeled in tokamak geometry taking into account nonlinear wave-particle interaction and the inhomogeneity of the distribution function on magnetic surfaces. The model includes self-consistently coupled beam tracing and Monte Carlo computations of the electron distribution function. The method of Green's function for the computation of the generated current is described. For the Axisymmetric Divertor Experiment Upgrade [Leuterer *et al.*, Fusion Eng. Des. **53**, 485 (2001)] parameters and high beam focusing, nonlinear wave-particle interaction effects appear to be important for perpendicular launch of the microwave beam and not important for oblique launches where they stay below the "threshold." With defocusing the beam two to three times along the direction of the magnetic field nonlinear effects of wave-particle interaction start to be important also for oblique launches. The effect of decreased current in case of increasing the microwave beamwidth is demonstrated. The decrease of both power absorption and generated current around low-order rational magnetic surfaces is found. Its possible effect on the tearing mode stability index is discussed. © *2005 American Institute of Physics*. [DOI: 10.1063/1.1823415]

I. INTRODUCTION

Electron cyclotron resonance heating (ECRH) and electron cyclotron current drive (ECCD) are standard methods of heating and sustainment of the stationary plasma current in toroidal fusion devices (tokamaks and stellarators). An important feature of these methods is the high localization of both power deposition and ECCD current profiles, which makes them useful for the control of the radial current profile. In particular, a very precise positioning of the generated current around a given magnetic surface is necessary for the suppression of neoclassical tearing modes (NTM) in tokamaks. Therefore, the accurate modeling of ECRH and ECCD is a practically important problem.

At the present time, such a modeling is performed in the framework of linear theory of wave propagation and absorption with the help of ray-tracing or beam-tracing methods, which are well justified by the fact that the parameter of geometrical optics, namely, the ratio of the wavelength to the characteristic scale of plasma or magnetic field inhomogeneity, is typically very small. In standard ECRH (ECCD) scenarii using the fundamental cyclotron resonance for the ordi-

nary wave mode (*O* mode) or the second harmonic resonance for the extraordinary wave mode (*X* mode), the wave propagation problem is solved using the cold plasma dielectric permittivity while thermal effects, which provide the correction to the permittivity responsible for the wave absorption, are taken into account by means of the wave absorption coefficient which is small compared to the wave vector. The expressions for this coefficient for the homogeneous Maxwellian plasma in a uniform magnetic field are used in most cases where ECRH/ECCD is modeled on the basis of linear theory.

The assumption that the electron distribution function is close to a Maxwellian is usually justified by the fact that, in off-axis heating scenarii, the magnetic surface average of the heating power per electron is small compared to the power exchanged by a given electron with other electrons via Coulomb collisions, which restore the Maxwellian distribution much faster than quasilinear effects distort it. However, this argument is not generally valid because it does not take into account the fact that power is highly localized both, in space, within the small interaction region on the magnetic surface

where the microwave beam crosses it, and in velocity space where the interaction is localized in a narrow resonance zone. There are two possibilities for the formation of essentially non-Maxwellian distribution functions in case of off-axis ECRH (ECCD).

The first of these possibilities is connected with the nonlinearity of wave-particle interaction within the beam, namely, with the trapping of resonant particles by the wave. In Ref. 1 it has been shown that this effect is important already in present day experiments with second harmonic *X*-mode ECRH. The nonlinearity can be roughly characterized by the nonlinear change of the wave-particle phase after a single pass of the particle through the microwave beam. In case of second harmonic *X*-mode resonance this parameter is given as $\epsilon_{NL} \sim (L_{\parallel}\omega/c)(E_0/B_0)^{1/2}\tan\chi$, where $L_{\parallel}$, ω, c, E_0, and B_0 are the parallel beamwidth, the wave frequency, the speed of light, the amplitude of both the wave electric field, and main magnetic field, respectively. Here $\tan\chi = v_{\perp}/v_{\parallel}$ is the tangent of the pitch angle. For the case of fundamental resonance for the *O* mode, $\epsilon_{NL} \sim (L_{\parallel}\omega/c)(E_0/B_0)^{1/2}\tan^{1/2}\chi$. For present day experimental parameters, for $\tan\chi \sim 1$, these parameters approach unity. In the reactor case, these parameters will be increased because of the increased beamwidth, and the increased magnetic field ($\omega \sim B_0$).

Another possibility for a strongly non-Maxwellian distribution function is given by ECRH (ECCD) in the vicinity of low-order rational magnetic surfaces (see Ref. 2). In this case, electrons leaving the microwave beam can reenter it several times after only a few toroidal rotations. Even if the nonlinearity is small $\epsilon_{NL} \ll 1$ the time between reentries is too short for Coulomb collisions to destroy small modifications of the distribution function caused by the wave. Thus, these modifications can accumulate during few successive electrons passes through the microwave beam along their "short path," leading to a significant deviation of the distribution function from a Maxwellian.

ECRH (ECCD) modeling in such cases must include, besides ray (beam) tracing, a separate procedure for the computation of wave absorption which is not described by linear theory anymore. This requires the computation of the electron distribution function. Based on a Monte Carlo method, such a procedure of the computation of the distribution function has been developed in Ref. 1. The main focus in that paper was on the proper description of the nonlinear wave-particle interaction with the microwave beam while the geometry of the main magnetic field outside the beam was assumed as simple as possible. In the present paper, a more realistic geometry of the tokamak magnetic field is considered. The problem of wave propagation in this geometry is solved using the beam tracing code TORBEAM,[3] which has been modified in order to use the nonlinear absorption coefficient obtained from the kinetic modeling with the Monte Carlo code ECNL. The problem geometry and the coupling of TORBEAM with ECNL are described in Sec. II.

In contrast to the precedent work[1] where only the perpendicular propagation of the wave beam with respect to the main magnetic field has been modeled, the general case of an arbitrary propagation angle is treated for midplane launching scenarii. Unlike the computation of absorbed power, the cal-

culation of the current driven by the wave is a more complicated problem whenever the electron distribution function *f* is modeled with a Monte Carlo method. Indeed, although the local changes in *f* in the resonance zone can be significant, the overall change of *f* remains very small: the average parallel electron velocity $V_{\parallel}$ is much smaller than the thermal velocity v_T. Therefore, the statistical noise appearing when modeling *f* results in large fluctuations in $V_{\parallel}$. In order to overcome this difficulty, similar to the method used in the linear theory of the current drive, a method for the computation of current using Green's function (current drive efficiency) has been implemented in ECNL. This method is discussed in Sec. III C.

Section IV presents the results of the modeling obtained for the Axisymmetric Divertor Experiment Upgrade[4] (AS-DEX Upgrade) parameters. In particular, as found in the modeling, the sensitivity of ECRH and ECCD to the presence of rational magnetic surfaces is demonstrated together with its effect on the tearing mode stability.

Finally, the applicability of both the model and the results of the modeling are discussed in Sec. V.

II. WAVE ABSORPTION IN A TOKAMAK GEOMETRY

For the computations using the TORBEAM-ECNL combination of codes, the analytic equilibrium model of the tokamak has been used,

$$R = R_0 + r\cos\theta - \Delta(r), \quad Z = r\kappa_e(r)\sin\theta, \tag{1}$$

where lines $r = $ const correspond to the poloidal cross-sections, $\varphi = $ const of the magnetic surfaces in cylindrical coordinates (R, Z, φ). Here, $\Delta(r)$ and $\kappa_e(r)$ are the Shafranov shift and the elongation, respectively. Temperature, density, and safety factor profiles are parabolic,

$$n_e = n_e(r) = n_0 + (n1 - n_0)\frac{r^2}{a^2}, \tag{2}$$

$$T_e = T_e(r) = T_{e0} + (T_1 - T_{e0})\frac{r^2}{a^2}, \tag{3}$$

$$q = q(r) = q_0 + (q_1 - q_0)\frac{r^2}{a^2}, \tag{4}$$

where *a* is the minor radius.

Within the beam-tracing model used in TORBEAM, the wave electric field is assumed in the form,

$$\tilde{\mathbf{E}}(\mathbf{r}, t) = A(\tau)\mathrm{Re}\,\mathbf{f}(\tau)\exp[is(\mathbf{r}, \tau) - \phi(\mathbf{r}, \tau) - i\omega t], \tag{5}$$

where τ is the reference ray parameter, $A(\tau)$ and $\mathbf{f}(\tau)$ are the wave amplitude and the polarization vector computed on the reference ray, $s(\mathbf{r}, \tau)$ and $\phi(\mathbf{r}, \tau)$ are the real and the complex phases, which describe the curvature of the wave front and the beam localization around the reference ray, and ω is the wave frequency, respectively. Here some renotation has been made as compared to Ref. 3. The parameter $\tau = \tau(\mathbf{r})$ is the solution to

$$[\mathbf{r} - \mathbf{q}(\tau)]\frac{d\mathbf{q}(\tau)}{d\tau} = 0, \tag{6}$$

where $\mathbf{q}(\tau)$ are the coordinates of the reference ray. In cases of interest, Eq. (6) has a unique solution in the vicinity of the reference ray $|\mathbf{r} - \mathbf{q}| \lesssim L_\perp$, where $L_\perp$ is a typical perpendicular beamwidth. The phases s and ϕ in Eq. (5) are represented by quadratic polynomial expansions over coordinates around the reference ray $\mathbf{r} - \mathbf{q}(\tau)$ such that the shape of the beam is Gaussian. In the standard approach of beam tracing, the wave absorption is taken into account in the amplitude which changes along the reference ray according to usual geometric optics,

$$\frac{dW}{dl} = -W\left(\frac{1}{v_g}\boldsymbol{\nabla} \cdot \mathbf{v}_g + \alpha\right), \tag{7}$$

$$W = \frac{|\widetilde{\mathbf{E}}|^2}{16\pi}\mathbf{f} * \cdot \left(\frac{1}{\omega}\frac{\partial}{\partial\omega}\omega^2\hat{\varepsilon}\right) \cdot \mathbf{f}, \tag{8}$$

where l is the distance counted along the reference ray, $\mathbf{v}_g$ is the group velocity, W is the wave energy density, and $\hat{\varepsilon}$ is the dielectric permittivity tensor of the cold plasma. In Eq. (7), α is the absorption coefficient,

$$\alpha = \frac{p_{abs}}{v_g W} = \frac{2\omega\mathbf{k} \cdot \mathbf{v}_g}{ckv_g}\kappa, \tag{9}$$

where p_{abs} is the absorbed power density, $\mathbf{k} = \boldsymbol{\nabla}s(\mathbf{r}, \tau)|_{\tau=\tau(\mathbf{r})}$ is the wave vector, c is the speed of light, and κ is the absorption index (imaginary part of the refraction index) obtained from the anti-Hermitian part of the dielectric permittivity tensor of the homogeneous plasma in a homogeneous magnetic field. Equation (7) approximates within geometrical optics the energy conservation law,

$$\boldsymbol{\nabla} \cdot \mathbf{S} + p_{abs} = 0, \tag{10}$$

where $\mathbf{S}$ is the Poynting vector,

$$\mathbf{S} \approx \mathbf{v}_g W = \frac{c|\widetilde{\mathbf{E}}|^2}{8\pi\omega}[\mathbf{k} - \text{Re}(\mathbf{fk} \cdot \mathbf{f}*)]. \tag{11}$$

As long as the linear relation (9) between α and p_{abs} is valid and the spatial scale of the absorption coefficient as well as the absorption length are much larger than the beamwidth, Eq. (7) represents the total power balance in the beam. The exact total power balance is obtained by integrating Eq. (10) over the volume between two surfaces which are close to each other and which are not tangential to the beam. For midplane off-axis ECCD scenarii with the resonance zone located on the high field side, a convenient choice for these surfaces is given by magnetic surfaces, which results in

$$\frac{dP_b(X)}{dX} = -\int_{-\pi}^{\pi}d\theta\int_{-\pi}^{\pi}d\varphi\sqrt{g}p_{abs}, \tag{12}$$

$$P_b \equiv \int_{-\pi}^{\pi}d\theta\int_{-\pi}^{\pi}d\varphi\sqrt{g}\mathbf{S} \cdot \boldsymbol{\nabla}X, \tag{13}$$

where $\sqrt{g}$ is the Jacobian of coordinates X, θ, φ. Here, the distance from the magnetic surface to the main torus axis,

$$X = X(r) = R_0 - r - \Delta(r) \tag{14}$$

is used instead of r as an independent variable for labeling the magnetic surfaces. Ignoring small variations of α and $\mathbf{v}_g$ within the beam in Eqs. (11) and (9) as well as such a variation of $\mathbf{v}_g \cdot \boldsymbol{\nabla}r$, one obtains

$$\frac{dP_b}{dX} = \frac{\alpha}{\cos\beta}P_b, \tag{15}$$

where β is the angle between the normal to the magnetic surface $\boldsymbol{\nabla}X$ and the group velocity at the intersection point of the reference ray with the surface.

The local relation (9) between the wave energy density and the absorbed power density is, strictly speaking, not valid even in linear theory because cyclotron absorption is an essentially nonlocal process: the energy coupled to the field by an electron in a given spatial point of the wave beam is determined by the interaction of this electron with the wave on its whole path through the beam. However, usually, the violation of the local relation is small as long as the change of the absorption coefficient within the beam due to the magnetic field variation along the field line is small as well as the uncertainty in this coefficient due to the finite width of the wave spectrum of parallel wave numbers $k_\parallel$. Thus, the influence of the absorption on the microwave beam profile across the beam can be ignored in this case. In case of the nonlinear wave-particle interaction, the influence of the absorption on the beam profile can be significant (see the discussion in Sec. VIII of Ref. 1). However, this influence will be ignored in the present study where wave absorption will be taken into account only in the total power conservation law (12) assuming that the results are qualitatively valid. In this context, Eq. (15) will be used as a definition of the absorption coefficient through the absorbed power calculated by the kinetic Monte Carlo code ECNL for a given value of the beam amplitude. Since such α is a nonlinear function of the beam amplitude, the computation of both the beam amplitude and absorbed power profiles over magnetic surfaces is performed by iterations until these profiles become consistent with each other.

III. KINETIC MODEL

A. Integral equation for the phase space flux density

For the computation of absorbed microwave power and generated current, the electron distribution function f is modeled using a Monte Carlo method. For this modeling, a tokamak with circular concentric magnetic surfaces is assumed. Test particles representing electrons are followed on the magnetic surfaces using a conventional Monte Carlo procedure. Whenever they are crossing the beam, their perpendicular velocity is randomly changed by a finite amount according to the nonlinear wave-particle interaction model of Ref. 1. The spatial regions where each of these models is used is separated by two poloidal cuts, A and B, located close
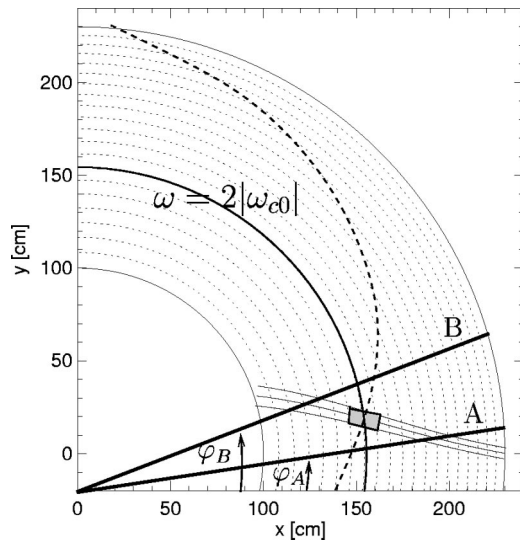
FIG. 1. Schematic location of the poloidal cuts A and B. The crossing of the cold cyclotron resonance line $\omega = 2|\omega_{c0}|$, with the magnetic field line (dashed curve) locates the resonance zone.

to each other (see Fig. 1). In the small inner region which contains the cross section of the beam with the magnetic surface, the kinetic equation is simplified to a Vlasov equation ignoring the Coulomb collision integral. In addition, the effect of the magnetic field inhomogeneity on electron orbits is neglected in this region. Namely, it is assumed that an electron entering this region through the point (X, θ) on one of the cuts moves in the uniform magnetic field $\mathbf{B}_0$ where $\mathbf{B}_0 = \mathbf{B}(\mathbf{r}_m)$ is the value of the tokamak main magnetic field at the point $\mathbf{r}_m = \mathbf{r}_m(X, \theta)$ in the inner region where the electron passes through the given wave electric field maximum on its orbit. Introducing the local Cartesian coordinate system with the z-axis directed along $\mathbf{B}_0$ and the x-axis directed along $\mathbf{k}_\perp = \{\boldsymbol{\nabla}s(\mathbf{r}, \tau) - [\boldsymbol{\nabla}s(\mathbf{r}, \tau) \cdot \mathbf{B}_0/B_0]\mathbf{B}_0/B_0\}|_{\tau=\tau_0}$, the microwave electric field is transformed to

$$\widetilde{\mathbf{E}} = E_0 \operatorname{Re} \mathbf{f} \exp\left[i(k_\perp x + k_\parallel z - \omega t) - \frac{z^2}{2L_\parallel^2} \right], \tag{16}$$

with the constants $k_\parallel = [\boldsymbol{\nabla}s(\mathbf{r}, \tau) \cdot \mathbf{B}_0/B_0]|_{\tau=\tau_0}$, $\mathbf{f} = \mathbf{f}(\tau_0)$,

$$E_0 = A(\tau_0)\exp\left[- \phi(\mathbf{r}_m, \tau_0)\right] = A(\tau_0)\exp\left(- \frac{r^2(\theta - \theta_0)^2}{2L_\perp^2}\right), \tag{17}$$

where τ_0 is the reference ray parameter at the intersection point with the magnetic surface and θ_0 is the poloidal coordinate of this point. Here the quadratic terms in the expansion of the real phase s around the reference ray have been neglected assuming the curvature of the phase front to be small. Moreover, both, parallel and perpendicular beamwidths $L_\parallel$ and $L_\perp$, which are defined by quadratic terms in the series expansion of the complex phase ϕ around the reference ray, have been replaced by their geometrical mean.

For the case of second harmonic X-mode propagation, the problem of electron motion in the uniform magnetic field

and the Gaussian microwave beam (16) has been reduced in Ref. 1 to a one-dimensional problem described by the Hamiltonian

$$\hat{H} = \Omega w - \tfrac{1}{2}w^2 + \varepsilon w e^{-\tau^2} \cos \psi, \tag{18}$$

where the dimensionless parameters are

$$\varepsilon = \frac{\sqrt{2}L_\parallel |k_\perp eE_0}{|v_\parallel|m_0\omega}|f_x - if_y|,$$

$$\Omega = \frac{\sqrt{2}L_\parallel}{|v_\parallel|}\left[k_\parallel v_\parallel - 2\omega_{c0}\left(1 - \frac{v_\parallel^2}{2c^2}\right) - \omega \right]. \tag{19}$$

The independent variables here are the dimensionless resonant perpendicular action, the wave-particle phase and the dimensionless time given by

$$w = \frac{\sqrt{2}L_\parallel |\omega_{c0}|v_\perp^2}{|v_\parallel|c^2}, \quad \psi = 2\phi_g + (k_\parallel v_\parallel - \omega)t + \psi_c, \quad \tau = \frac{|v_\parallel|t}{\sqrt{2}L_\parallel}, \tag{20}$$

respectively. Here, e, m_0, $v_\perp$, $v_\parallel$, ϕ_g, and ψ_c are the electron charge, the rest mass, the perpendicular and the parallel velocity, the gyrophase, and the constant phase shift, respectively, and $\omega_{c0} = eB_0/(m_0c) < 0$ is the nonrelativistic electron cyclotron frequency. The change of the parallel velocity of electrons is negligibly small in the inner region.[1]

Using the fact that particles entering the inner region have a random distribution over the phase ψ_c, the solution to the Vlasov equation obtained with the help of the method of characteristics can be transformed to an integral relation between the gyroaveraged pseudoscalar flux densities of electrons entering the beam, Γ^{in} and of electrons leaving the beam, Γ^{out} (see Ref. 1),

$$\Gamma^{\text{out}}(X, \theta, v_\perp, v_\parallel) = \int_0^\infty dv_\perp' P^H(v_\perp, v_\perp')\Gamma^{\text{in}}(X, \theta, v_\perp', v_\parallel). \tag{21}$$

Here, the incoming flux density,

$$\Gamma^{\text{in}} = \frac{J|V_\parallel^\varphi|}{2\pi}\int_{-\pi}^\pi d\phi_g f = \frac{\Delta N}{2\pi\Delta X\Delta\theta\Delta v_\perp \Delta v_\parallel\Delta t}, \tag{22}$$

where

$$J = \sqrt{g}v_\perp, \quad V_\parallel^\varphi = v_\parallel\frac{B^\varphi}{B}, \quad B^\varphi = \mathbf{B} \cdot \boldsymbol{\nabla}\varphi \tag{23}$$

are the Jacobian of phase space coordinates and the contravariant toroidal component of the parallel velocity, respectively, is calculated on cut A for particles with $v_\parallel > 0$ and on cut B for particles with $v_\parallel < 0$. Here, Γ^{in} is also expressed through the number of electrons passing through the element of the cut $\Delta X\Delta\theta$ in the velocity range $\Delta v_\perp \Delta v_\parallel$ per time interval Δt (see also Ref. 5). In the definition of the outgoing flux density Γ^{out} cuts A and B should be swapped. The transition probability density (TPD) P^H, which describes the change of the perpendicular velocity of electrons due to their nonlinear interaction with the microwave beam, is

$$P^H(v_\perp, v'_\perp) = \frac{\partial w}{\partial v_\perp} \frac{\partial v'_\perp}{\partial w'} \mathcal{P}^D_{AB}(w, w') = \frac{v_\perp}{v'_\perp} \mathcal{P}^D_{AB}(w, w'), \quad (24)$$

where $w = w(v_\perp)$ and $w' = w(v'_\perp)$ are given by Eq. (20) and the discretized TPD $\mathcal{P}^D_{AB}$ is given by Eq. (60) of Ref. 1. In the following, the relation (21) will used also in the symbolic operator form,

$$\Gamma^{\text{out}} = \hat{P}^H \Gamma^{\text{in}}. \quad (25)$$

The dependencies of the discretized TPD $\mathcal{P}^D_{AB}$ on parallel velocity, beam and magnetic field parameters enter this function only through the dimensionless parameters ε and Ω [Eq. (19)]. Therefore, for the purpose of Monte Carlo modeling, this quantity has been precalculated in the whole parameter range except in the regions where the nonlinearity parameter,

$$\epsilon_{NL} = \sqrt{\varepsilon \Omega} \approx \frac{\omega L_\|}{c} \sqrt{\frac{N_\perp E_0}{2 B_0}} \frac{v_\perp}{|v_\||} \quad (26)$$

is very small (there the quasilinear approximation is used) or very large (there the adiabatic model is used), see Ref. 1. Here $N_\perp = c k_\perp / \omega \sim 1$ is the perpendicular refraction index.

In the outer region (which is the region delimited by the cuts A and B and not containing the cross section of the beam with the magnetic surface) the amplitude of the beam is exponentially small and, therefore, the wave electromagnetic field is neglected there. Moreover, the tokamak geometry is simplified for the modeling of the distribution function in this region. Namely, in a computation with a given X value in Eq. (12) the magnetic surfaces are assumed to be circular and concentric around the magnetic axis located at $R = R_s \equiv R_0 - \Delta[r(X)]$ where $r(X)$ is the solution to Eq. (14). The small radius of quasitoroidal coordinates $(\rho, \vartheta, \varphi)$ associated with this axis, coincides with $r(X)$ on the considered surface, but differs from r on the nearby surfaces labeled with X' so that $X' = R_s - \rho = X - r(X) + \rho$. Thus, the Jacobian of coordinates (X, θ, φ) coincides with the Jacobian of quasitoroidal coordinates, $\sqrt{g} = \rho R = \rho(R_s + \rho \cos \vartheta)$, on the reference ray $\vartheta = \pi$. The cross-field transport, the momentum conservation during collisions, and the toroidal inhomogeneity of the magnetic field are ignored in the outer region defined above. The kinetic equation corresponding to this model has the form

$$\frac{\partial f}{\partial t} + \frac{v_\|}{q R_s} \frac{\partial f}{\partial \vartheta} + \frac{v_\|}{R_s} \frac{\partial f}{\partial \varphi} = \hat{L}_{CM} f. \quad (27)$$

Here, $\hat{L}_{CM}$ is the Coulomb collision operator for isotropic Maxwellian background particles and q is the safety factor. In steady state, the formal solution to Eq. (27) can, again, be expressed through the relation between Γ^{out} and Γ^{in},

$$\Gamma^{\text{in}} = \hat{P}^O \Gamma^{\text{out}}, \quad (28)$$

which explicitly reads

$$\Gamma^{\text{in}}(X, \vartheta, v_\perp, v_\|)$$
$$= \int_{-\pi}^{\pi} d\vartheta' \int_0^\infty dv'_\perp \int_{-\infty}^\infty dv'_\| P^O(\vartheta, v_\perp, v_\|; \vartheta', v'_\perp, v'_\|)$$
$$\times \Gamma^{\text{out}}(X, \vartheta', v'_\perp, v'_\|), \quad (29)$$

where

$$P^O(\vartheta, v_\perp, v_\|; \vartheta', v'_\perp, v'_\|) = P_t(v_\perp, v_\|; v'_\perp, v'_\|) [\delta(\vartheta - \vartheta')$$
$$- 2\pi/q) \Theta(v'_\|) + \delta(\vartheta - \vartheta')$$
$$+ 2\pi/q) \Theta(-v'_\|)]$$
$$+ P_r(v_\perp, v_\|; v'_\perp, v'_\|) \delta(\vartheta - \vartheta'). \quad (30)$$

Here $P_t(v_\perp, v_\|; v'_\perp, v'_\|)$ is the transition probability density from the velocity space point $v'_\perp, v'_\|$ to the point $v_\perp, v_\|$ in the case that the particle traverses the outer region, $v'_\| v_\| > 0$, $P_r(v_\perp, v_\|; v'_\perp, v'_\|)$ is such a TPD in the case that the particle returns to the starting cut, $v'_\| v_\| < 0$ and Θ is the Heaviside step function. Combined together, relations (25) and (28) provide a homogeneous integral equation for the flux density

$$\Gamma^{\text{out}} = \hat{P}^H \hat{P}^O \Gamma^{\text{out}}. \quad (31)$$

It should be noted that for midplane heating scenarii with the resonance zone located on the high field side, the effect of toroidicity in the outer region does not have a significant influence on the distribution function in the resonance zone located in the passing particle region of the velocity space. However, this effect as well as the momentum conservation during Coulomb collisions is important for the generated current. The procedure taking these effects into account in the computation of the current is described in Sec. III C.

B. Monte Carlo algorithm

The formal solution to Eq. (31) is

$$\Gamma^{\text{out}} = \lim_{K \to \infty} \frac{1}{K} \sum_{k=1}^{K} (\hat{P}^H \hat{P}^O)^k F, \quad (32)$$

where a particular choice for F is $F = C_n \delta(X - X_0) \delta(\vartheta - \vartheta_0) \delta(v_\perp - v_{\perp 0}) \delta(v_\| - v_{\|0})$ and C_n is a normalization constant (F can be an arbitrary integrable function of phase space variables). This formal solution can be presented as an expectation value of the test particle density on the cut averaged over the Markov chain,

$$\Gamma^{\text{out}}(X, \vartheta, v_\perp, v_\|)$$
$$= C_n \delta(X - X_0) \lim_{K \to \infty} \frac{1}{K}$$
$$\times \sum_{k=1}^{K} \overline{\delta(\vartheta - \vartheta_k^{\text{out}}) \delta(v_\perp - v_{\perp k}^{\text{out}}) \delta(v_\| - v_{\|k}^{\text{out}})}, \quad (33)$$

where the chain is determined by the following recurrence relations (the variable X remains unchanged),

$$\vartheta_k^{\text{out}} = \vartheta_k^{\text{in}}, \quad \vartheta_k^{\text{in}} = \vartheta_{k-1}^{\text{out}} + \frac{2\pi}{q}\text{sgn}(v_{\|k}^{\text{in}})\Theta(v_{\|k}^{\text{in}}v_{\|k-1}^{\text{out}}), \tag{34}$$

$$v_{\perp k}^{\text{out}} = V_\perp^H(\vartheta_k^{\text{in}},v_{\perp k}^{\text{in}},v_{\|k}^{\text{in}}), \quad v_{\perp k}^{\text{in}} = V_\perp^O(v_{\perp k-1}^{\text{out}},v_{\|k-1}^{\text{out}}), \tag{35}$$

$$v_{\|k}^{\text{out}} = v_{\|k}^{\text{in}}, \quad v_{\|k}^{\text{in}} = V_\|^O(v_{\perp k-1}^{\text{out}},v_{\|k-1}^{\text{out}}), \tag{36}$$

and the initial condition $\vartheta_0^{\text{in}} = \vartheta_0$, $v_{\perp 0}^{\text{in}} = v_{\perp 0}$, $v_{\|0}^{\text{in}} = v_{\|0}$. Here, the superscripts "in" and "out" on the variables indicate the incoming and outgoing flux regions, respectively, and $V_\perp^H$, $V_\perp^O$, and $V_\|^O$ are random numbers defined by the following expectation values:

$$\overline{\delta(v_\perp - V_\perp^H(\vartheta,v_\perp',v_\|))} = P^H(v_\perp,v_\perp'), \tag{37}$$

$$\overline{\delta(v_\perp - V_\perp^O(v_\perp',v_\|'))\delta(v_\| - V_\|^O(v_\perp',v_\|'))}$$
$$= P_t(v_\perp,v_\|;v_\perp',v_\|')\Theta(v_\|v_\|') + P_r(v_\perp,v_\|;v_\perp',v_\|')\Theta(-v_\|v_\|'). \tag{38}$$

The small change of ϑ due to the rotational transform in the inner region is ignored in Eq. (34). The sampling of $V_\perp^H(\vartheta,v_\perp',v_\|)$ using the known TPD $P^H(v_\perp,v_\perp')$ is standard

(see, e.g., Ref. 6). As for $V_\perp^O(v_\perp',v_\|')$ and $V_\|^O(v_\perp',v_\|')$, these quantities are obtained using a conventional Monte Carlo procedure for solving the drift-kinetic equation.[7] Starting the orbit of a test particle with the velocities $(v_\perp',v_\|')$ in the outgoing flux region of the respective cut and following its random walk until it hits one of the cuts at a location in the incoming flux region, $V_\perp^O(v_\perp',v_\|')$ and $V_\|^O(v_\perp',v_\|')$ are obtained as the values of $v_\perp$ and $v_\|$ at the hit point, respectively. It should be noted that, due to a simplified tokamak geometry, the conventional Monte Carlo method[7] requires only a few steps per sampling of these quantities in the long mean free path regime. The case of a realistic geometry will be considered in future using the technique of Ref. 5 which has similar efficiency.

The limit of zero toroidicity, $\rho/R_s \to 0$, used in the transition probabilities (38) will not be used for the derivations presented in the following, where the final formulas are independent of toroidicity.

The normalization constant C_n in Eq. (33) is determined by the expression for the particle density n averaged over the volume between two close magnetic surfaces (such averages are referred as flux surface averages in the following),

$$n_e(X) \equiv \frac{1}{4\pi^2\Delta X}\left(\int_{-\pi}^{\pi}d\vartheta\sqrt{g}\right)^{-1}\int_{X-\Delta X/2}^{X+\Delta X/2}dX'\int_{-\pi}^{\pi}d\vartheta\int_{-\pi}^{\pi}d\varphi\sqrt{g}n(X',\vartheta,\varphi)$$
$$= \frac{1}{2\pi\rho R_s\Delta X}\int_{X-\Delta X/2}^{X+\Delta X/2}dX'\int_{-\pi}^{\pi}d\vartheta\int_0^\infty dv_\perp\int_{-\infty}^\infty dv_\|\Gamma^{\text{out}}(X',\vartheta,v_\perp,v_\|)\overline{\Delta t(v_\perp,v_\|)}, \tag{39}$$

where $\overline{\Delta t(v_\perp,v_\|)}$ is the average time it takes for a particle leaving the region of the beam with the velocity $(v_\perp,v_\|)$ to reenter this region. The sample of this quantity Δt_k is obtained as a by-product when sampling $v_{\perp k+1}^{\text{in}}$ and $v_{\|k+1}^{\text{in}}$ within a conventional random walk procedure. Substituting Eq. (33) in Eq. (39) and replacing there $\overline{\Delta t(v_{\perp k}^{\text{out}},v_{\|k}^{\text{out}})}$ with Δt_k, one obtains

$$n_e = \frac{C_n}{2\pi\rho R_s\Delta X}\lim_{K\to\infty}\frac{1}{K}\sum_{k=1}^K\overline{\Delta t_k}. \tag{40}$$

ECRH power absorption can be characterized by the total absorbed power density in the layer between two close magnetic surfaces [see Eq. (12)]. It is given by the difference between the incoming and the outgoing kinetic energy fluxes within the layer,

$$\frac{dP_b(X)}{dX} = \frac{2\pi}{\Delta X}\int_{X-\Delta X/2}^{X+\Delta X/2}dX'\int_{-\pi}^{\pi}d\vartheta\int_0^\infty dv_\perp\int_{-\infty}^\infty dv_\|$$
$$\times [\Gamma^{\text{in}}(X',\vartheta,v_\perp,v_\|) - \Gamma^{\text{out}}(X',\vartheta,v_\perp,v_\|)]\frac{m_0v^2}{2}. \tag{41}$$

Substituting in Eq. (41) the expression for the outgoing flux

density (33) and also the following expression for the incoming flux density,

$$\Gamma^{\text{in}}(X,\vartheta,v_\perp,v_\|)$$
$$= C_n\delta(X - X_0)\lim_{K\to\infty}\frac{1}{K}$$
$$\times\sum_{k=1}^K\overline{\delta(\vartheta - \vartheta_k^{\text{in}})\delta(v_\perp - v_{\perp k}^{\text{in}})\delta(v_\| - v_{\|k}^{\text{in}})}, \tag{42}$$

one obtains with the account of Eq. (40)

$$\frac{dP_b(X)}{dX} = 2\pi^2\rho R_s m_0 n_e\lim_{K\to\infty}$$
$$\times\left(\sum_{k=1}^K\overline{\Delta t_k}\right)^{-1}\sum_{k=1}^K\overline{[(v_{\perp k}^{\text{in}})^2 - (v_{\perp k}^{\text{out}})^2]}. \tag{43}$$

It should be noted that essential contributions to the second sum in Eq. (43) come only when the test particle passes through the resonance zone which is very narrow both in coordinate space, where it is limited by the beam region, and in velocity space. Moreover, the location of this resonance zone in velocity space is usually in the high energy region scarcely visited by test particles. Therefore, the variance in

the absorbed power would be very large if one would directly use the simple Monte Carlo procedure described here. Hence, this procedure has been complemented by a weight windows technique based on a splitting-roulette algorithm and has been applied, in particular, in Ref. 8 for the computation of high energy "tails" of the minority ion distribution function during ion cyclotron heating.

C. Green's function method for the current density

The parallel current density,

$$
j_\parallel = \frac{e}{\rho R \Delta X} \int_{X-\Delta X/2}^{X+\Delta X/2} \mathrm{d}X' \int_{-\pi}^{\pi} \mathrm{d}\vartheta \int_0^\infty \mathrm{d}v_\perp
$$
$$
\times \int_{-\infty}^\infty \mathrm{d}v_\parallel \, \mathrm{sgn}(v_\parallel) \Gamma^{\mathrm{out}}(X',\vartheta,v_\perp,v_\parallel) \frac{B(X',\vartheta)}{B^\varphi(X',\vartheta)}, \quad (44)
$$

can also be computed in a straightforward way,

$$
j_\parallel = 2\pi e n_e \frac{R_s}{R} \lim_{K\to\infty} \left(\sum_{k=1}^K \overline{\Delta t_k} \right)^{-1} \sum_{k=1}^K \overline{\mathrm{sgn}(v_{\parallel k}^{\mathrm{out}}) \frac{B(X,\vartheta_k^{\mathrm{out}})}{B^\varphi(X,\vartheta_k^{\mathrm{out}})}}, \quad (45)
$$

where it has been used that $j_\parallel/B$ is constant on the magnetic surface. However, such a method gives a large relative variance in the result as compared to such a variance in the absorbed power density. This large variance comes from taking into account in the expression for the current the complete distribution function where the current generated by particles with $v_\parallel > 0$ is almost compensated by the current generated by particles with $v_\parallel < 0$. Since both these large contributions have statistical errors, the resulting current is strongly polluted by statistical noise. Much better results are obtained using a precomputed current drive efficiency which also allows to take into account the toroidal magnetic field inhomogeneity and momentum conservation during Coulomb collisions of nonresonant bulk electrons determining the current.

For this purpose, the kinetic equation is rewritten in guiding center variables $\mathbf{z} = \mathbf{z}(\mathbf{r},\mathbf{p}) = (\mathbf{x},v_\perp,v_\parallel)$ and ϕ_g where $\mathbf{x}$ are some curvilinear spatial coordinates of the guiding center being (X,ϑ,φ) in this case,

$$
\frac{\partial f}{\partial t} + V^i \frac{\partial f}{\partial z^i} - \omega_c \frac{\partial f}{\partial \phi_g} - \hat{L}_C f = Q^H, \quad (46)
$$

$$
Q^H \equiv -e\left(\tilde{\mathbf{E}} + \frac{1}{c}\mathbf{v}\times\tilde{\mathbf{B}}\right) \cdot \frac{\partial z^i}{\partial \mathbf{p}} \frac{\partial f}{\partial z^i}, \quad (47)
$$

where $V^i = \dot{z}^i$ are equations of guiding center motion, $\mathbf{v}$ and $\mathbf{p}$ are the particle velocity and the kinematic momentum, respectively, and $\tilde{\mathbf{B}}$ is the wave magnetic field. Assuming Q^H to be known, neglecting the contribution of the cross-field drift in V^i, linearizing the collision integral and averaging Eq. (46) over time and gyrophase one obtains a stationary drift-kinetic equation with a source term,

$$
V_\parallel^i \frac{\partial f}{\partial z^i} - \hat{L}_{CL} f = \langle\langle Q^H\rangle_t\rangle_{\phi_g}. \quad (48)
$$

The linearization of the collision integral here is justified because the distribution function can strongly differ from the Maxwellian only in the resonance zone and in the high energy region of the velocity space. The amount of electrons in these regions is small. Therefore, the contribution of these electrons to the Coulomb diffusion coefficients which are integral moments of f can be treated as a linear perturbation. The solution of Eq. (48) in terms of Green's function gives for the current the following expression (compare to Ref. 9):

$$
\frac{j_\parallel}{B} \int \mathrm{d}^3x \sqrt{g} B = \int \mathrm{d}^3x \sqrt{g} j_\parallel = 2\pi e \int \mathrm{d}^5z J v_\parallel f
$$
$$
= 2\pi e \int \mathrm{d}^5z JG \langle\langle Q^H\rangle_t\rangle_{\phi_g}, \quad (49)
$$

where the following short notation has been introduced for the integrals,

$$
\int \mathrm{d}^3x \equiv \int_{X-\Delta X/2}^{X+\Delta X/2} \mathrm{d}X' \int_{-\pi}^{\pi} \mathrm{d}\vartheta \int_{-\pi}^{\pi} \mathrm{d}\varphi,
$$

$$
\int \mathrm{d}^5z \equiv \int \mathrm{d}^3x \int_0^\infty \mathrm{d}v_\perp \int_{-\infty}^\infty \mathrm{d}v_\parallel. \quad (50)
$$

In Eq. (49), $G(X,\vartheta,v_\perp,v_\parallel)$ is the generalized Spitzer–Härm function which satisfies the adjoint kinetic equation

$$
V_\parallel^i \frac{\partial}{\partial z^i} G f_M + \hat{L}_{CL} G f_M = -v_\parallel f_M, \quad (51)
$$

where f_M is a Maxwellian. Since the wave electromagnetic field in the source term (47) is negligible in the outer region, the integration over φ in the last expression in Eq. (50) can be reduced to the inner region. In this inner region the collision integral can be ignored in Eq. (46) when expressing f in Eq. (47) through its value on the boundary ($\varphi=\varphi_A$ for cut A or $\varphi=\varphi_B$ for cut B). For this purpose, the solution of the Vlasov equation resulting from Eq. (46) using the method of characteristics has been used in Ref. 1. Ignoring in this Vlasov equation the cross-field drift, replacing the poloidal variable ϑ with the field aligned variable $\theta=\vartheta+(\varphi-\varphi_A)/q$ and the velocity space variables $v_\perp$ and $v_\parallel$ with the integrals of drift motion $\mu=v_\perp^2/2B$ and $\mathcal{E}=(v_\perp^2+v_\parallel^2)/2$ and rewriting it in the form of a conservation law, after time and gyrophase averaging, the source term is expressed as

$$
\langle\langle Q^H\rangle_t\rangle_{\phi_g} = \frac{1}{J'}\frac{\partial}{\partial\varphi} J' V_\parallel^\varphi \frac{1}{2\pi}\int_{-\pi}^{\pi} \mathrm{d}\phi_g \langle f\rangle_t, \quad (52)
$$

where $J' = JB/(v_\perp|v_\parallel|)$. Substituting Eq. (52) in Eq. (50), where the integration variables have also to be swapped, performing the integration over φ between the cuts and ignoring the small variation of G along the drift orbit (with φ variable) caused by collisions in favor of the variation of f, one obtains

$$j_\parallel = eB \left(\Delta X \int_{-\pi}^{\pi} \mathrm{d}\vartheta \sqrt{g}B \right)^{-1} \int_{X-\Delta X/2}^{X+\Delta X/2} \mathrm{d}X' \int_{-\pi}^{\pi} \mathrm{d}\vartheta$$

$$\times \int_{0}^{\infty} \mathrm{d}v_\perp \int_{-\infty}^{\infty} \mathrm{d}v_\parallel G(X',\vartheta,v_\perp,v_\parallel)[\Gamma^{\mathrm{out}}(X',\vartheta,v_\perp,v_\parallel)$$

$$- \Gamma^{\mathrm{in}}(X',\vartheta,v_\perp,v_\parallel)]. \tag{53}$$

Here, the variables have been swapped back after the integration over φ and the definition of flux densities (22) has been used. In analogy with Eq. (41), the current density can be expressed in terms of Markov chain variables,

$$j_\parallel = en_e \frac{B}{B_a} \lim_{K\to\infty} \left(\sum_{k=1}^{K} \overline{\Delta t_k} \right)^{-1}$$

$$\times \sum_{k=1}^{K} \overline{[G(X,\vartheta_k^{\mathrm{out}},v_{\perp k}^{\mathrm{out}},v_{\parallel k}^{\mathrm{out}}) - G(X,\vartheta_k^{\mathrm{in}},v_{\perp k}^{\mathrm{in}},v_{\parallel k}^{\mathrm{in}})]}, \tag{54}$$

where

$$\frac{1}{B_a} = \frac{1}{2\pi} \int_{-\pi}^{\pi} \frac{\mathrm{d}\vartheta}{B}. \tag{55}$$

In the following, the flux surface average of $j_\parallel$ obtained by putting in Eq. (53) $B=B_a$ will be used. The function G has been precomputed for the long mean free path regime using the method of Ref. 10 and has been used in Monte Carlo calculations in the form of interpolation. This allowed to reduce the relative variance in the current to the level of such a variance in the absorbed power.

IV. RESULTS OF THE MODELING

A. Midplane off-axis ECRH and ECCD

The modeling with the TORBEAM-ECNL combination of codes has been performed for beam and plasma parameters in the range of interest at ASDEX upgrade. Plasma major and minor radii, the magnetic field strength on the axis, central and edge values of the electron density, the temperature, and the safety factor profiles [see Eqs. (2)–(4)] are $a=65$ cm, $R_0=165$ cm, $B_{axis}=2.1$ T, $n_0=6\times10^{13}$ cm^{-3}, $n_1 =10^{12}$ cm^{-3}, $T_0=2.4$ keV, $T_1=0.24$ keV, $q_0=1$, and $q_1=4$, respectively. The wave frequency $\omega/2\pi=140$ Ghz corresponds to the second harmonic resonance located at the high field side, $1\leqslant\kappa_e(r)\leqslant1.5$, -10 cm $\leqslant\Delta(r)\leqslant5$ cm. The input power is $P=0.5$ MW. The case of low field side launch in the midplane is considered. The initial width of the microwave beam 2.97 cm and the initial focusing $1/R_f =1/129.4$ cm results in an average beamwidth in the absorption zone of $(L_\parallel L_\perp)^{1/2}=3$ cm. Two specific toroidal launching angles, $\phi_{inj}=0°$ and $\phi_{inj}=-10°$ (this leads to 70° angle between the magnetic field and group velocity in the absorption region, see Fig. 1) has been chosen for the investigations.

In the first case, as in the earlier computations for the Wendelstein 7-AS stellarator (W7-AS) parameters,[1] nonlinear effects reduce the absorption coefficient significantly, leading to the broadening and radial shift of the absorbed power density profile (see Fig. 2). At the same time, nonlinear effects are not significant in the second case for the nor-
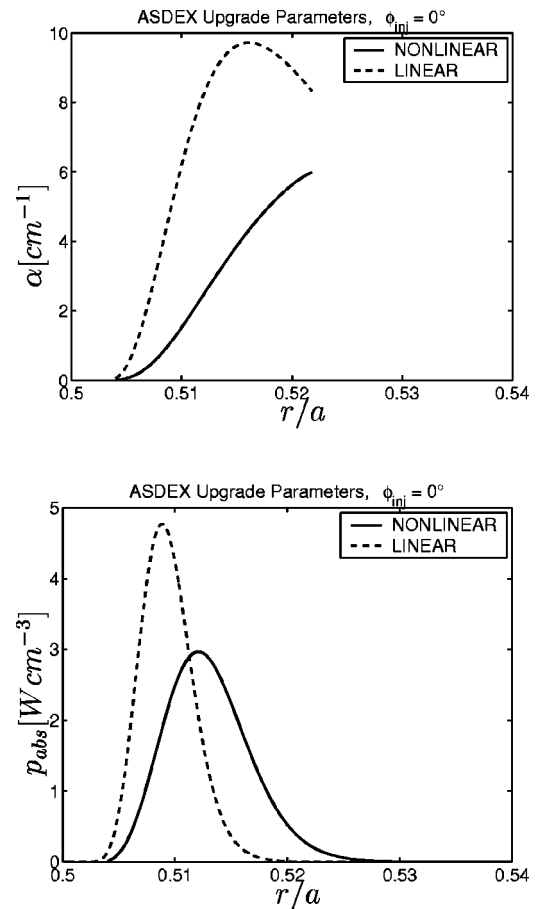

FIG. 2. Absorption coefficient α and surface averaged absorbed power density p_{abs} as functions of the dimensionless radius r/a for the case of perpendicular launch. Solid—nonlinear model, dashed—linear model. The "cold" resonance $\omega=2|\omega_{c0}|$ is located at $r/a=0.503$.

mally focused beam (see Fig. 3). Moreover, the effects of plateau formation are also not important for this off-axis ECCD scenario. However, the linear model stays here right on the margin of the applicability region. This can be seen from Fig. 4 where the nonlinearity parameter (26) averaged with the exchanged power density in velocity space,

$$\overline{\epsilon_{NL}} \equiv \lim_{K\to\infty} \left(\sum_{k=1}^{K} \overline{|(v_{\perp k}^{\mathrm{in}})^2 - (v_{\perp k}^{\mathrm{out}})^2|} \right)^{-1}$$

$$\times \sum_{k=1}^{K} \overline{\epsilon_{NL}(\vartheta_k^{\mathrm{in}},v_{\perp k}^{\mathrm{in}},v_{\parallel k}^{\mathrm{in}})|(v_{\perp k}^{\mathrm{in}})^2 - (v_{\perp k}^{\mathrm{out}})^2|} \tag{56}$$

is shown together with the surface averaged absorbed power density as a function of the relative parallel beamwidth $L_\parallel/L_{\parallel0}$ in the point of maximum linear absorption. For this $L_\parallel$ scan, the power in the beam in the maximum point of absorption is kept unchanged and equal to 500 kW. With increasing $L_\parallel/L_{\parallel0}$ the nonlinear reduction of the absorbed power causes a reduction in the local current density (see Fig. 3), while, as far as the beam does not get too narrow such that the parallel spectral width becomes comparable with $k_\parallel$, the magnitude of $L_\parallel/L_{\parallel0}$ has no effect on the linear calculation, where an instantaneous redistribution of the absorbed power along the field lines is assumed. The total
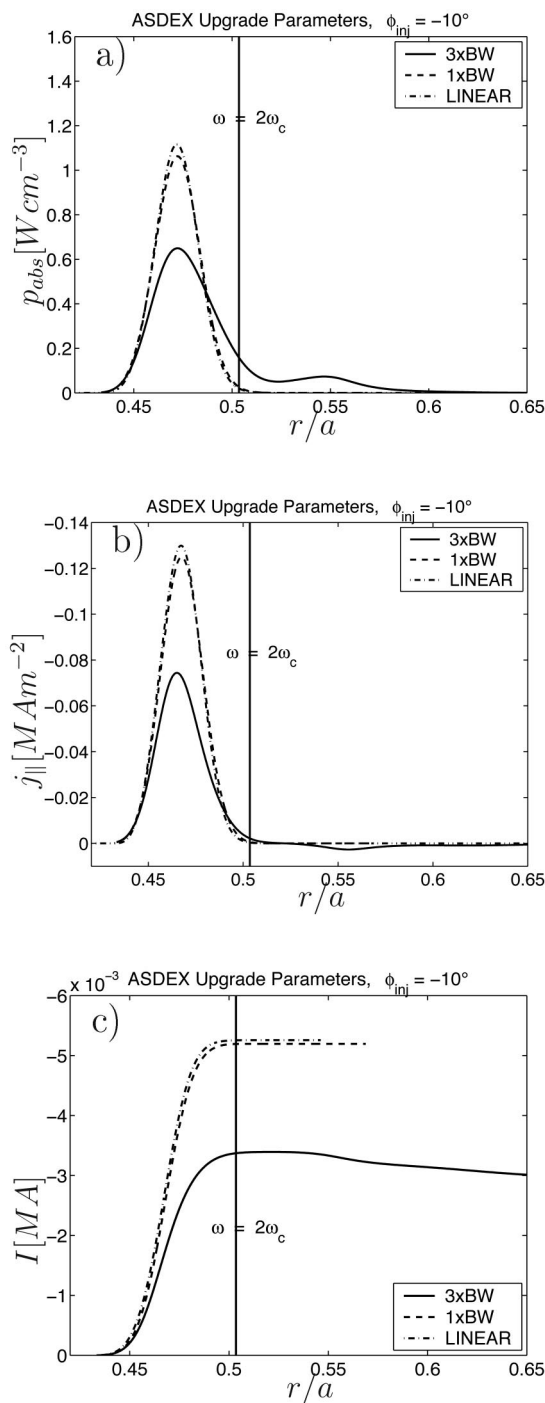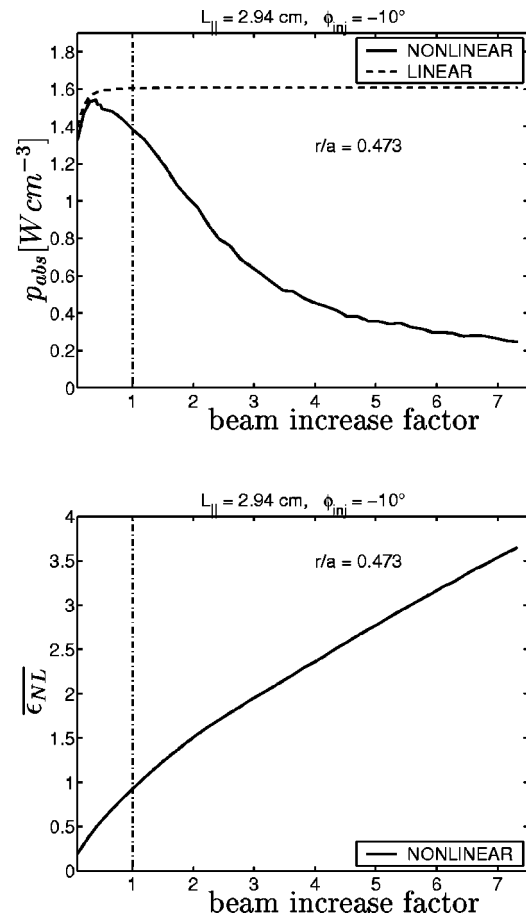
FIG. 4. Dependencies of p_{abs} for the nonlinear and linear models (top) and average nonlinearity parameter (56) $\overline{\epsilon_{NL}}$ (bottom) on the relative parallel beam width $L_{\parallel}/L_{\parallel 0}$ where $L_{\parallel 0}$ is a beam width given by TORBEAM.

FIG. 3. Surface averaged absorbed power density p_{abs}, surface averaged parallel current density $j_{\parallel}$, and total driven current I as functions of the dimensionless radius r/a for the toroidal injection angle $\phi_{inj}=-10°$. The position of cold resonance $\omega=2|\omega_{c0}|$ is shown with solid vertical line. Indications $1\times$BW and $3\times$BW correspond to the nonlinear model with normal parallel beam width $L_{\parallel}$ and $L_{\parallel}$ increased three times keeping the same input power in the beam, respectively.

B. ECCD near rational magnetic surfaces

Changing in the ASDEX upgrade parameter set of Sec. IV A B_{axis} and T_0 to 2.157 T and 5 keV, respectively, the power deposition profile for the launching angle $\phi_{inj}=-10°$ is centered around the low order rational magnetic surface with $q=3/2$. The same localization is retained in case where n_0 is reduced by a factor of 6, T_0 is increased by a factor of 3, and B_{axis} is increased to $B_{axis}=2.19$ T so that the effects of
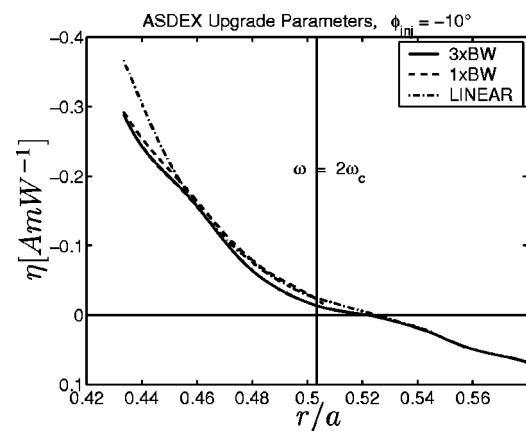
value of the current is also reduced due to the shift of the absorption profile towards the cold resonance zone where the local current drive efficiency defined as a ratio of surface averaged current and absorbed power densities $\eta=j_{\parallel}/p_{abs}$ is smaller. The change of η from the linear value is not large in all cases (see Fig. 5).

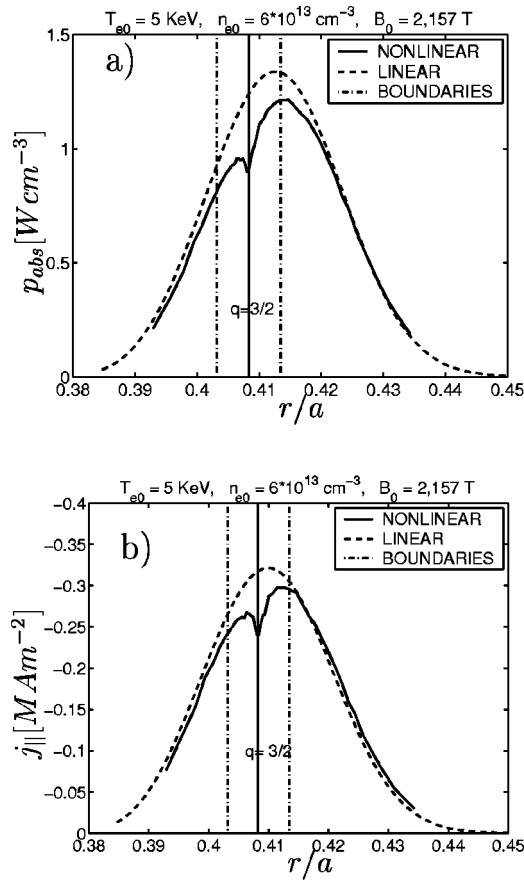FIG. 5. Current drive efficiency η for cases shown in Fig. 3.

FIG. 6. Surface averaged absorbed power density p_{abs} (a) and surface averaged parallel current density $j_\parallel$ (b) as functions of the dimensionless radius r/a for the nonlinear and linear models. Cold resonance position and boundaries of region (57) are shown with solid and dashed-dotted vertical lines, respectively.

FIG. 7. The same as Fig. 6 for the extreme long mean free path regime (cf. Sec. IV B).

the formation of the plateau on the distribution function and the consequent quasilinear degradation of absorption and current drive become significant. In both these cases shown in Figs. 6 and 7, the reduction of the absorbed power density p_{abs} and of the generated current density $j_\parallel$ can be seen around a rational magnetic surface in the region where q satisfies the inequality

$$\left| q - \frac{M}{N} \right| \leq \Delta q_{cr} = \frac{qL_\parallel}{2\pi r N}. \tag{57}$$

Boundaries of this region where the field line can reenter the beam at least once after $M=3$ toroidal revolutions are shown in these figures with dashed-dotted vertical lines. In the second case, the quasilinear degradation of absorption and current drive can be seen also on irrational magnetic surfaces. The reduction of the absorption can be clarified considering the distribution function on two magnetic surfaces whose positions are shown with short solid vertical lines in Fig. 7(a). Comparing the distribution function at two different spatial points of the magnetic surface within the region (57) on cut A (incoming flux region), namely, in the region of the beam $\vartheta = \pi$ and away from the beam $\vartheta \approx 3\pi/2$ one can observe a much more distinct plateau on f at the point $\vartheta = \pi$ where electrons return to the beam after M turns (see Fig. 8).
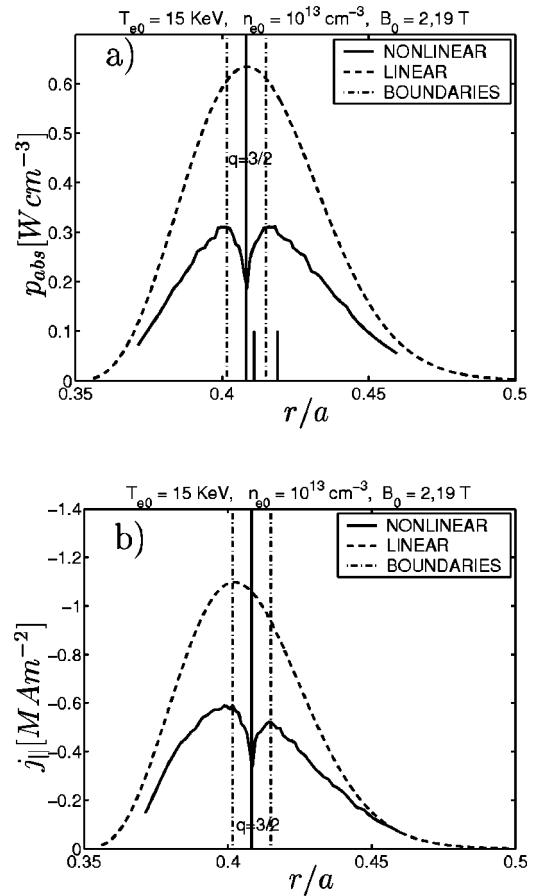
This is better seen in Fig. 9 where the distribution function is shown as a function of the perpendicular velocity for a fixed value of the parallel velocity (distributions along dashed lines in Fig. 8). In this figure, the distributions for $\vartheta = \pi$ on the other side of the beam where resonant electrons are leaving it are also shown.

The poloidal asymmetry of f can also be seen on the magnetic surface located outside the region (57) (Fig. 10). Such an asymmetry comes from the fact that the relaxation time of the distribution function in velocity space remains comparable with the relaxation time over the magnetic surface even in the extreme long mean free path regime. The first of these mentioned relaxation times is the Coulomb diffusion time across the resonance zone in velocity space τ_{rc}. The width of this zone is determined either by the broadening of the cyclotron resonance line due to the spectral width of the beam, or by the broadening due to nonlinear effects $\Delta v_\perp \sim \max[c^2 v_\parallel / (\omega L_\parallel v_\perp), c(E_0/B_0)^{1/2} \ll v_\perp]$. Thus, $\tau_{rc} = \Delta v_\perp^2 / (\nu_c v^2)$ where ν_c is a collision frequency. The relaxation time over the irrational magnetic surface is roughly a return time to the beam $\tau_{rms} = 4\pi^2 R_0 r / (L_\perp v_\parallel)$, which is larger than the toroidal bounce time by a factor $2\pi r / L_\perp \gg 1$. These times appear to be comparable in the considered "extreme" case (with $\Delta v_\perp / v \sim 0.1$, $\nu_e \sim 2 \times 10^3$ s^{-1}, $v \sim 6 \times 10^9$ cm s^{-1}, and $r = 26$ cm one has $\tau_{rc} \sim 5 \times 10^{-6}$ s and $\tau_{rms} \sim 10^{-5}$ s), while in more realistic cases the first of them
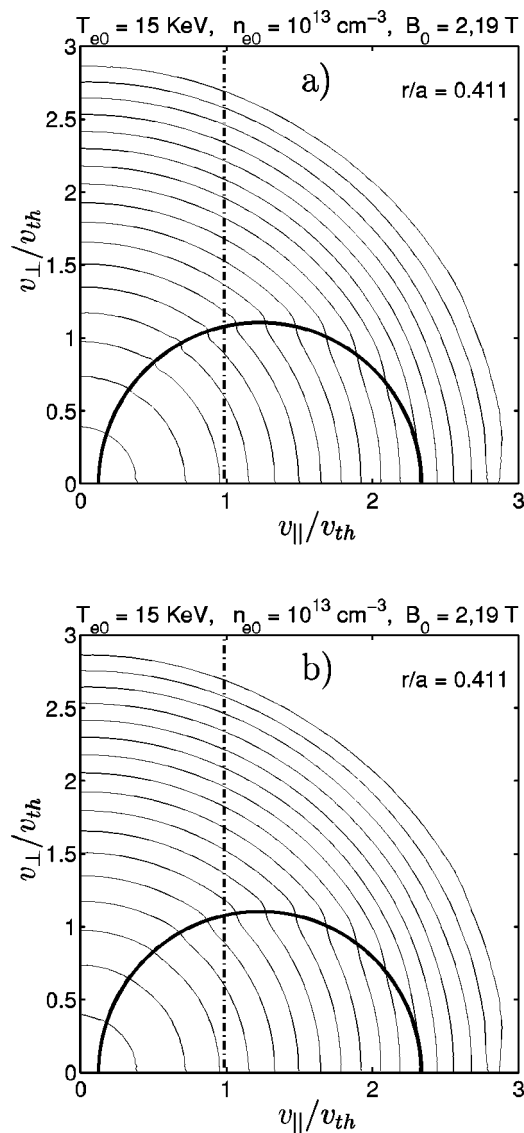
FIG. 8. Contour lines of the electron distribution function on entry of the beam for the magnetic surface within the region (57) for $\vartheta = \pi$ (a) and $\vartheta \approx 3\pi/2$ (b). The thick half circular line is the cyclotron resonance line $\omega = k_\parallel v_\parallel - 2\omega_{c0}[1 - v^2/(2c^2)]$. Stronger quasilinear effect in the beam region is observable through the stronger distorsion of contours on plot (a) around the resonance line as compared to plot (b).

is smaller. Therefore, the electron distribution function is essentially a four-dimensional function on magnetic surfaces in case of off-axis heating scenarii.

As it is known,[11] the stability of the tearing mode can be influenced using ECCD around rational magnetic surfaces because modifications of current around these surfaces modify the value of the tearing mode stability index Δ'. The presence of a relatively small dip on the ECCD current profile exactly at the rational surface is able to change the situation dramatically. Calculations of Δ' in the cylindrical approximation of the tokamak with the toroidal current taken as a sum of the Ohmic current corresponding to the q profile (4) and ECCD currents shown in Fig. 6(b) give for the stability index without ECCD $\Delta' = -0.055$ cm^{-1}. With co- and counter-ECCD calculated using the linear absorption model (no dip), $\Delta' = -3.3$ cm^{-1}, and $\Delta' = 1.9$ cm^{-1}, respectively. At
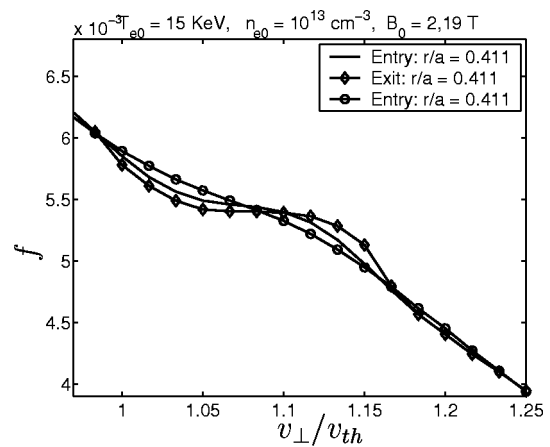

FIG. 9. Electron distribution function over perpendicular velocities on the magnetic surface within the region (57) $r/a = 0.411$. The corresponding value of $v_\parallel/v_{th} = 1$ is shown in Fig. 8 with dashed-dotted line. Line with no markers—distribution on entry of the beam at $\vartheta = \pi$, diamonds—$\vartheta = \pi$ on exit of the beam, circles—$\vartheta \approx 3\pi/2$ (region with no beam). The distribution of electrons which enter the beam (entry) exhibits a much more pronounced plateau around the resonance zone for $\vartheta = \pi$ as compared to $\vartheta \approx 3\pi/2$ (see also Fig. 8). The distribution on the other side of the beam (Exit) where resonant electron are leaving is the most perturbed.

the same time, the current profile with a dip given by the nonlinear model results in $\Delta' = 5.1$ cm^{-1} and $\Delta' = -1$ cm^{-1} for co- and counter-ECCD, respectively, i.e., the sign of Δ' is changed to the opposite, as compared to the linear model.

V. DISCUSSION AND CONCLUSIONS

The modeling of off-axis midplane ECRH and ECCD in a tokamak has been performed with taking into account the effects of nonlinear wave-particle interaction and the inhomogeneity of the electron distribution function on the magnetic surface, but neglecting the radial transport of electrons. For this purpose, a kinetic Monte Carlo code ECNL has been developed and coupled with the beam tracing code TORBEAM. The Green's function method applied in ECNL for the calculations of ECCD current allowed to take into ac-
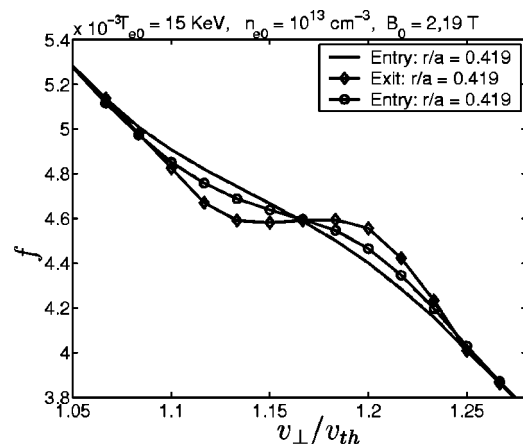

FIG. 10. The same as in Fig. 9 for the magnetic surface located outside the region (57) $r/a = 0.419$. The difference in distributions on entry (poloidal asymmetry) is due to the fact that relaxation times in velocity space and over the magnetic surface are comparable.

count momentum conservation and toroidicity in the case of a simple test particle dynamics. In addition, it reduces the statistical errors in the current to the levels of such an error in the absorbed power.

Within the Monte Carlo model, a few approximations have been made. In particular, Coulomb collisions have been ignored in the inner region. Their effect on the wave-particle interaction can be estimated using the decorrelation function $\delta\Phi$ introduced in Ref. 12 and in its relativistic form in Ref. 13. This function is proportional to the variance in the wave-particle phase during the interaction time. Using the estimate

$$\delta\Phi \sim \frac{\nu_c}{\omega}\frac{v}{c}\left(L_\parallel\frac{\omega}{c}\right)^3, \tag{58}$$

for the parameter values $\nu_c = 4 \times 10^4$ s^{-1}, $L_\parallel = 3$ cm, $v/c = 0.1$, and $\omega \approx 8.10^{11}$ s^{-1}, one obtains $\delta\Phi \sim 10^{-3}$. Therefore, the effect of collisions on wave-particle interaction is negligibly small. However, for very wide beams $L_\parallel \gtrsim 30$ cm this effect would become increasingly important. The influence of cross-field transport on the deformation of the distribution function in the resonance zone has also been neglected because it is small compared to the effect of Coulomb collisions. For the estimate, relating the change of the cyclotron resonance condition,

$$\omega - 2\omega_{c0}\left(1 + \frac{v^2}{c^2}\right) - k_\parallel v_\parallel = 0, \tag{59}$$

due to radial diffusion affecting ω_{c0} to its change due to collisional diffusion, one obtains $(\nu_c R_0^2/D_\perp)^{-1/2}/\max(v^2/c^2, N_\parallel v/c)$, which is typically smaller than one. Here $D_\perp$ is the radial diffusion coefficient. The effect of plasma rotation, which has also been neglected in the model, is small as long as the plateau establishment time τ_{rc} is small compared to the time needed for a toroidal plasma displacement by one beamwidth $\tau_\varphi = L_\parallel/V_{E\varphi}$, where $V_{E\varphi} \sim qR_0 v_T^2/(a^2\omega_{c0})$. In the considered cases, $\tau_{rc}/\tau_\varphi \sim 0.1$. In addition, toroidal trapping of electrons does not play a decisive role in the process of plateau formation in ECCD scenarii with midplane heating in the case of a resonance zone location on the high field side which is of interest here.

The modeling for ASDEX upgrade parameters shows that the reduction of the absorption coefficient and the broadening of the absorbed power density profile due to nonlinear effects is significant for heating scenarii with injection angles close to perpendicular. At the same time, in the ECCD scenario with a well focused beam ($L_\parallel = 3$ cm) both nonlinear effects and the quasilinear distortion of the distribution function are not significant. However, when increasing the microwave beam size by a factor 3 in the parallel direction while keeping the same input power in the beam, nonlinear effects become important. They reduce the absorption coefficient and shift the power deposition profile towards the region with lower current drive efficiency. Therefore, nonlinear effects could be observed from the total value of ECCD current which is reduced for such a defocused beam.

It should be mentioned that nonlinear reduction of the absorption of perpendicularly injected microwave beams has been observed on the W7-AS stellarator.[14] In these experiments an increase in the power transmitted after a single pass of the beam through a low density plasma has been measured as compared to the predictions of linear theory. At the same time, detailed measurements of the ECCD efficiency on the DIII-D tokamak,[15] a device of the same scale as ASDEX upgrade, show a good agreement of these measurements with the predictions of linear and quasilinear theory.

Note that the onset of nonlinear effects is linked more with an increase of the microwave beam cross section rather than with an increased power in the beam. This can be seen from the nonlinearity parameter ϵ_{NL}, Eq. (26), which weakly scales with power as $P^{1/4}$ while its scaling with the beam-width is $L_\parallel^{3/4}L_\perp^{-1/4}$. The positive scaling with $L_\parallel$ is due to the fact that for larger $L_\parallel$ the increase in the electron interaction time with the beam prevails over the reduction of the wave amplitude and leads, as a result, to a larger nonlinear shift of the wave-particle phase. The scaling with the pitch angle $\epsilon_{NL} \sim \tan\chi$ indicates that nonlinear effects are less significant if the main power absorption is done by strongly passing particles. In present day experiments with well focused beams $\epsilon_{NL} \lesssim 1$ for $\tan\chi = 1$. At the same time, in ECCD scenarii, particles with $\tan\chi < 1$ play the main role in the absorption, especially if β_e is high. Linear and quasilinear theory are well applicable in this velocity space region, what, in particular, has been confirmed for DIII-D parameters by direct computations of electron orbits in the wave electromagnetic field in Ref. 16. However, in a reactor-scale device, this velocity space region will shrink due to increased $\epsilon_{NL} > 1$ at $\tan\chi = 1$ owing to larger beam widths, larger main magnetic field ($\epsilon_{NL} \sim B_0^{1/2}$) and higher power in the beam.

In the vicinity of low order rational magnetic surfaces, the quasilinear effect becomes important. It leads to the formation of a plateau on the electron distribution function and a consequent reduction of power absorption and generated current there. As a result, current profiles with a dip on the rational surface are created. The presence of such a dip can change the sign of the tearing mode stability index Δ' to the opposite as compared to the profile following from linear theory which is without a dip. Hence cocurrent drive becomes destabilizing and countercurrent drive becomes stabilizing. This conclusion, however, shows only the tendency in the considered parameter range because the effect of the cross-field radial transport of current-carrying electrons is not taken into account in the computation. Roughly, radial transport would smear the current over the radial scale $\delta r \sim (D_\perp/\nu_{cs})^{1/2}$ where ν_{cs} is the collision frequency for supra-thermal resonant electrons. The process of radial relaxation of current carriers occurs on a much longer time scale (of the order of the current destruction time) than the process of plateau formation which takes place on a time scale of the order of collisional diffusion time across the narrow resonance zone in velocity space. Estimating $\nu_{cs} \sim 2 \times 10^4$ s^{-1} and $D_\perp \sim 10^4$ cm^{2}s^{-1} one obtains $\delta r \sim 0.7$ cm which is comparable with 0.8 cm being the half-width of the region (57) containing the dip on the current profile (see Figs. 6 and 7). Though, such an estimate might use too large values of anomalous $D_\perp$. The formation of transport barriers around low order rational magnetic surfaces in ECRH heated plasmas on the Rijnhuizen Tokamak Project[17] (RTP) suggests

lower values of anomalous transport there. In particular, as shown in Ref. 18, the anomalous transport caused by a small scale magnetic perturbations can be strongly reduced around low order rational magnetic surfaces. As shown above, the radial transport is not important for the plateau formation. Therefore, the toroidal asymmetry of the distribution function and, respectively, of the electron cyclotron emission would not be affected by the cross-field transport. Note that incomplete relaxation of the distribution function over near-rational magnetic surfaces has been considered in Ref. 19 as one of the possible reasons for the toroidal asymmetry of electron cyclotron emission in ECRH experiments on RTP. At the same time, practically interesting cases where the effect of the reduction of ECCD current near rational surfaces can influence the tearing mode stability index are still to be found. The possible existence of such cases could provide a method for NTM stabilization which does not need an active control of the ECCD current profile. Indeed, if a rather broad radial profile of the ECCD current is created, it can cover the whole region where the low order rational surface is expected and the dip on the current profile is automatically formed around this surface, thus preventing the growth of NTMs up to large saturation levels. As shown experimentally in Ref. 20 where the ECCD cocurrent was created before the mode onset at the radial position where the NTM was expected, preventing the NTM at the initial stage needs less ECCD power than stabilizing a developed NTM. The efficiency of such a method depends on the accuracy of the ECCD current profile placement to a resonant magnetic surface. Therefore, possible automatic profile placement would be of interest.

ACKNOWLEDGMENTS

[1]R. Kamendje, S. V. Kasilov, W. Kernbichler, and M. F. Heyn, Phys. Plasmas **10**, 75 (2003).
[2]R. O. Dendy, Plasma Phys. Controlled Fusion **27**, 1243 (1985).
[3]E. Poli, A. G. Peeters, and G. V. Pereverzev, Comput. Phys. Commun. **136**, 90 (2001).
[4]F. Leuterer, M. Beckmann, and H. Brinkschulte, Fusion Eng. Des. **53**, 485 (2001).
[5]S. V. Kasilov, W. Kernbichler, V. V. Nemov, and M. F. Heyn, Phys. Plasmas **9**, 3508 (2002).
[6]M. H. Kalos and P. A. Whitlock, *Monte Carlo Methods. Volume I: Basics* (Wiley, New York, 1986).
[7]A. H. Boozer and G. Kuo-Petravic, Phys. Fluids **24**, 851 (1981).
[8]S. V. Kasilov, V. E. Moiseenko, M. F. Heyn, and W. Kernbichler, in *12th Topical Conference on Radio Frequency Power in Plasmas, Savannah, Georgia, 1997*, AIP Conf. Proc. No. 403 (AIP, Woodbury, NY, 1997), pp. 321–324.
[9]T. Antonsen and K. Chu, Phys. Fluids **25**, 1295 (1982).
[10]S. V. Kasilov and W. Kernbichler, Phys. Plasmas **3**, 4115 (1996).
[11]E. Westerhof, Nucl. Fusion **27**, 1929 (1987).
[12]S. V. Kasilov, A. I. Pyatak, and K. N. Stepanov, in *Reviews of Plasma Physics*, edited by B. B. Kadomtsev (Consultants Bureau, New York, 1997), Vol. 20.
[13]S. V. Kasilov, in *Proceedings of the Seventh European Fusion Theory Conference*, edited by A. Rogister (Forshungszentrum Jülich GmbH, Jülich, Germany, 1998), pp. 111–114.
[14]H. P. Laqua, V. Erckmann, W7-AS Team, and ECRH-Group, in *31st EPS Conference on Plasma Physics, London, 28 June–2 July* (EPS, Petit-Lancy, 2004), Vol. 28B, pp. P-1.209.
[15]C. C. Petty, R. Prater, J. Lohr, T. C. Luce, W. R. Fox, R. W. Harvey, J. E. Kinsey, L. L. Lao, and M. A. Makowski, Nucl. Fusion **42**, 1366 (2002).
[16]R. W. Harvey and R. Prater, in *Radio Frequency Power in Plasmas: 14th Topical Conference* (AIP, New York, 2001), pp. 298–301.
[17]G. M. D. Hogeweij, N. J. Lopes-Cardozo, M. R. De-Baar, and A. M. R. Schilham, Nucl. Fusion **38**, 1881 (1998).
[18]S. V. Kasilov, D. Reiter, A. M. Runov, W. Kernbichler, and M. F. Heyn, Plasma Phys. Controlled Fusion **44**, 985 (2002).
[19]J. A. Konings, A. G. Peeters, G. M. D. Hogeweij, and E. Westerhof, in *Proceedings of the Ninth Joint Workshop on Electron Cyclotron Emission and Electron Cyclotron Heating, Borrego Springs, California, 23–26 January 1995* (World Scientific, Singapore, 1995).
[20]K. Nagasaki, A. Isayama, S. Ide, and JT-60 team, Nucl. Fusion **43**, L7 (2003).